ELSEVIER

L-band Microwave Emission of the Biosphere (L-MEB) Model: Description and calibration against experimental data sets over crop fields

J.-P. Wigneron [a,*], Y. Kerr [b], P. Waldteufel [c], K. Saleh [a], M.-J. Escorihuela [b], P. Richaume [b], P. Ferrazzoli [d], P. de Rosnay [b], R. Gurney [e], J.-C. Calvet [f], J.P. Grant [g], M. Guglielmetti [h], B. Hornbuckle [i], C. Mätzler [j], T. Pellarin [k], M. Schwank [h]

[a] *INRA, EPHYSE, Villenave d'Ornon, France*
[b] *CESBIO, Toulouse, France*
[c] *IPSL/Service d'Aéronomie, Paris, France*
[d] *Universita di Roma Tor Vergata, Roma, Italy*
[e] *NERC, University of Reading, Reading, UK*
[f] *METEO-FRANCE/CNRM, Toulouse, France*
[g] *Vrije Universiteit Amsterdam, The Netherlands*
[h] *ETH, Zürich, Switzerland*
[i] *Iowa State University, Ames, USA*
[j] *IAP, University of Bern, Switzerland*
[k] *LTHE, Grenoble, France*

Abstract

In the near future, the SMOS (Soil Moisture and Ocean Salinity) mission will provide global maps of surface soil moisture (SM). The SMOS baseline payload is an L-band (1.4 GHz) two dimensional interferometric microwave radiometer which will provide multi-angular and dual-polarization observations. In the framework of the ground segment activities for the SMOS mission an operational SMOS Level 2 Soil Moisture algorithm was developed. The principle of the algorithm is to exploit multi-angular data in order to retrieve simultaneously several surface parameters including soil moisture and vegetation characteristics. The algorithm uses an iterative approach, minimizing a cost function computed from the differences between measured and modelled brightness temperature (T_B) data, for all available incidence angles.

In the algorithm, the selected forward model is the so-called L-MEB (L-band Microwave Emission of the Biosphere) model which was the result of an extensive review of the current knowledge of the microwave emission of various land covers. This model is a key element in the SMOS L2 algorithm and could be used in future assimilation studies. There is thus a strong need for a reference study, describing the model and its implementation. In order to address these needs a detailed description of soil and vegetation modelling in L-MEB is given in this study. In a second step, the use of L-MEB in soil moisture retrievals is evaluated for several experimental data sets over agricultural crops. Calibrations of the soil and vegetation L-MEB parameters are investigated for corn, soybean and wheat. Over the different experiments, very consistent results are obtained for each vegetation type in terms of calibration and soil moisture retrievals.
© 2006 Elsevier Inc. All rights reserved.

Keywords: Passive microwave; SMOS; Soil; Vegetation; Soil moisture; Modelling; Inversion; Algorithm; L-MEB

1. Introduction

L-band (1.1–1.7 GHz) microwave radiometry is one of the most relevant remote sensing techniques to monitor soil moisture

---

* Corresponding author.
 E-mail address: wigneron@bordeaux.inra.fr (J.-P. Wigneron).

over land surfaces at the global scale (Jackson et al., 1999; Kerr, in press; Njoku et al., 2003; Schmugge, 1998). Two proposed space missions, SMOS (Soil Moisture and Ocean Salinity, Kerr et al., 2001), and Hydros (Hydrosphere State, Entekhabi et al., 2004) are based on that technique in order to obtain global maps of the surface soil moisture in the near future. The SMOS mission was proposed to the European Space Agency in the framework of the Earth Explorer Opportunity Missions in 1998; it is planned for a launch in 2007. The baseline SMOS payload is an L-band (1.4 GHz) two dimensional (2-D) interferometric radiometer that is Y shaped with three 4.5 m arms. SMOS aims at providing global maps of soil moisture, with an accuracy better than 0.04 m^3/m^3 every 3 days, with a space resolution better than 50 km (Kerr et al., 2001).

As the satellite moves over the Earth, a given point within the Field Of View (FOV) is observed from different view angles by the 2-D interferometer. The series of dual-polarized multi-angular measurements allow simultaneous retrievals of several surface parameters including soil moisture and vegetation optical depth (Wigneron et al., 2001). As part of the SMOS mission, geophysical products such as soil moisture (SM) and vegetation opacity (τ) will be produced by an operational algorithm. The principle of the algorithm is based on an iterative approach, minimizing a cost function computed from the sum of squared weighted differences between measured and modelled microwave brightness temperature (T_B) data, for a variety of incidence angles (Kerr et al., 2006). In the algorithm, for each incidence angle, the different cover types (bare soil and vegetated area, open water, urban area, etc.) present within the SMOS footprint are estimated from high resolution land use maps. For low vegetation and forest categories, these maps used a large number of sub-categories corresponding, for instance, to grasslands, crops, scrubs, tropical and boreal forests, which were distinguished for a variety of climatic and geographic conditions. Currently, the ECOCLIMAP data base (Masson et al., 2003) that distinguishes 218 ecosystems at 1 km resolution was selected as the reference landcover map. Within each pixel, the brightness temperatures from each cover type are simulated with a forward model and then aggregated, accounting for the SMOS field of view and antenna pattern. Parameters driving the forward model are selected and tabulated based on the selected vegetation classes and on maps of soil properties (for soil texture, roughness and bulk density). This manuscript will only describe the forward model used over each homogeneous vegetation type and the description of the whole algorithm and of the aggregation process over heterogeneous pixels is described in Kerr et al. (2006). The forward model selected is the so-called L-MEB (L-band Microwave Emission of the Biosphere; Wigneron et al., 2003) model which was used in the first ESA studies aiming at evaluating SMOS capabilities from synthetic data sets (Pellarin et al., 2003a,b,c). The L-MEB model was the result of an extensive review of the current knowledge of the microwave emission of various land cover types (herbaceous and woody vegetation, frozen and unfrozen bare soil, etc.), with the objective of being accurate while remaining simple enough for operational use at global scale and while allowing developments to be incorporated as they occur.

Since the first version of L-MEB, a large number of experimental campaigns have been carried out for a variety of vegetation/soil characteristics and climatic conditions (De Rosnay et al., 2006a; Fenollar et al., 2006; Grant et al., 2007; Hornbuckle et al., 2003; Schwank et al., 2005). Combined experimental and modelling activities have contributed to improving very significantly our knowledge of the key processes that drive the emission of the soil and vegetation canopy such as rainfall interception within the canopy, mulch and litter in prairies and forests, surface roughness, effective soil temperature, dependence of vegetation attenuation on configuration parameters (incidence angle, polarization), etc. These results were integrated in L-MEB. As L-MEB is the forward model used in the processing of the SMOS level-2 soil moisture products, it may also be used in assimilation studies of microwave brightness temperature observations developed by assimilation centres (Dirmeyer & Gao, 2004; Seuffert et al., 2003). There is thus a strong need for a study describing L-MEB in detail and providing key information for model calibration over a variety of vegetation types.

The objective of this study is to describe the new version of L-MEB and analyse its calibration and validation over cropped fields. First, a reference description of L-MEB will be given, including key results which have contributed to recent improvements of the model. The focus of the present paper is on vegetation canopies with low levels of biomass and soil; the case of forests will be the subject of another paper. Second, the calibration and validation of L-MEB will be investigated from SM retrievals using experimental data sets over cropped fields. L-MEB calibration over grassland was investigated separately in another paper (Saleh et al., submitted for publication).

2. Model description

2.1. General

Over a given pixel, a large variety of vegetation types may happen to be present; for instance wheat, sorghum and fallow, deciduous and coniferous forests. To simplify the algorithm process, the land use classes, as defined by land cover maps at high (1 km) resolution, were grouped into a smaller number (about 10) of generic classes having the same modelling characteristics and similar parameters. These generic classes correspond to bare soil and low vegetation covers, forests, wetlands, water, barren areas, frozen soils, snow covered areas, ice, urban and built-up areas. The SM retrievals are carried out only over the area within the pixel corresponding to bare soil and low vegetation covers (referred to as the nominal class) and some forested areas. Within those areas, the contributions of the dominant vegetation types to the surface microwave emission are summed accounting for their cover fraction (defined at a 4 km spatial resolution currently) and the antenna pattern. The contributions of the other generic classes are computed using ancillary information and simplified modelling approaches.

It would not be possible to describe in detail in this paper the modelling approaches selected for all the different land cover types considered in ECOCLIMAP. This paper will only

Table 1
Main references for experimental and modelling studies considered in the development of L-MEB, listed as a function of the generic land cover classes used in the Level-2 algorithm

Land cover types	Experimental and theoretical studies (data bases and model evaluation)	L-MEB Modelling
Nominal class (bare soil and low vegetation cover)		This issue
-Bare soil	• This issue • PORTOS-93 (Wigneron et al., 2003) • SMOSREX (De Rosnay et al., 2006a; Escorihuela et al., submitted for publication) • SMMR data (Pellarin et al., 2006) • Schwank and Mätzler (2006) • Schneeberger et al. (2004) • Shi et al. (2005)	Wigneron et al. (2006b)
-Cropland	•This issue • BARC (Wang et al., 1982) • PORTOS-91, 93, EMIRAD, (Wigneron et al., 1995, 2004) • REBEX (Hornbuckle et al., 2003)	Wigneron et al. (2006a)
-Grassland	• Saleh et al. (submitted for publication) • SMOSREX (De Rosnay et al., 2006a) • Schwank et al. (2005)	Saleh et al. (submitted for publication)
Forest		Ferrazzoli et al. (2002) Della Vecchia et al. (in press)
-Coniferous	• EuroSTARRS (Della Vecchia et al., 2006; Saleh et al., 2004) • BRAY-04 (Grant et al., 2007)	Ferrazzoli et al. (2002)
-Deciduous broadleaf	• Jülich data (Guglielmetti et al., submitted for publication) • Ferrazzoli and Guerriero (1996)	Della Vecchia et al. (in press)
-Evergreen broadleaf	• SMMR data (Pellarin et al., 2006)	
Wetlands	no specific data set or modelling	
Water	Mätzler et al. (2006)	
Barren or sparsely vegetated areas	• MELBEX (Fenollar et al., 2006)	
Frozen soils	• Hallikainen et al. (1984) • Mätzler, 1993, 2006 • SMOSREX (De Rosnay et al., 2006a) • Schwank et al. (2004)	Wigneron et al. (2006a)
Snow covered areas	• Pulliainen and Hallikainen (2001) • Mätzler, 2001; Mätzler et al., 2006 • DOMEX 2004, Macelloni et al., 2006	Wigneron et al. (2006a)
Ice	• Mätzler, 2001; Mätzler et al., 2006	
Urban areas	• EuroSTARRS, Toulouse urban site (Lopez-Baeza et al., 2003)	

describe in detail the modelling approach selected for the nominal class (low vegetation and bare soil). References for field studies and modelling activities associated to the other vegetation types and generic classes are summarized in Table 1. Modelling for forests is summarized in Section 2.4.

As for topography, it seems that excluding steep terrain in mountainous areas, it has relatively low effects on T_B (Kerr et al., 2003; Pellarin et al., 2006). Therefore, topography effects are not modelled in L-MEB and the proposed approach in the L2 algorithm is to process a global Digital Elevation Model (DEM) so as to compute a descriptor of the topography (topography index) for the whole pixel. The index is compared to three thresholds corresponding to three main levels of topography effects (1) high: the area is flagged as highly mountainous and no retrievals are attempted (2) moderate: SM retrievals are carried out but a caution flag indicates the presence of moderate topography (3) low: it is estimated that topography will not affect the retrieved SM values. Default values of the thresholds are yet to be estimated and they will be refined after analysis of actual SMOS observations.

The brightness temperature of a mixed pixel will be denoted T_{BP}, where the subscript 'P' is for polarization (P=V for vertical and P=H for horizontal). As described above, it is written as a linear combination of the brightness temperature of each land cover, weighted by their respective cover fraction within the pixel and accounting for the actual characteristics of the SMOS antenna pattern (Kerr et al., 2006). As described in the literature (Ulaby et al., 1981–1986), upward atmospheric emission ($T_{B-SKY-U}$) and atmospheric attenuation (parameterized by the atmospheric optical thickness τ_{ATM}) must be taken into account for simulating top-of-the-atmosphere $T_B(T_{BP\_TOA})$:

$$T_{BP\_TOA} = T_{BP} \exp(-\tau_{ATM}/\cos(\theta)) + T_{B-SKY-U} \tag{1}$$

where T_{BP} is the brightness temperature at the surface level, i.e. as observed immediately above the canopy. A simplified approach, described by Pellarin et al. (2003a), was developed in L-MEB to compute τ_{ATM} and $T_{B-SKY-U}$. In the following, we will focus our analysis on the modelling of T_{BP} for bare soil and low vegetation.

2.2. Soil modelling

2.2.1. Soil reflectivity

The soil microwave emission (T_{B-GP}) is generally written as a function of the ground emissivity (e_{GP}) and the effective soil temperature (T_G) (Ulaby et al., 1981–1986):

$$T_{B-GP} = e_{GP} \cdot T_G \tag{2}$$

The effective soil temperature (T_G) accounts for the fact that T_{B-GP} is a weighted sum of the emission from layers at subsurface levels, which have different characteristics in terms of physical temperature and emissivity. Soil emissivity is generally computed as one minus soil reflectivity ($e_{GP}=1-r_{GP}$), where r_{GP} is the integral of the surface scattering effects over the upper hemisphere. For smooth soil surfaces and homogeneous soils, the soil microwave reflectivity (r_{GP}) can be approximated from the soil reflectivity (r^*_{GP}) of a plane surface:

$$r_{GP} \approx r^*_{GP} = |R_P(\varepsilon_G, \theta)|^2 \tag{3}$$

where the reflection coefficient (R_P) can be calculated from the soil dielectric permittivity (ε_G) and the incidence angle θ, using the Fresnel equations ($R_P = R_P(\varepsilon_G, \theta)$). For soils, ε_G is mainly determined by the soil moisture content and, to a somewhat smaller extent, by soil density, textural and structural properties. Modelling of T_G and ε_G will be analysed in detail in the following sections.

Natural surfaces are not flat generally and soil roughness effects have to be taken into account. The reflectivity (r_{GP}) of a rough surface is generally written as the sum of two components: the non-coherent (r_{GP}^{non}) and the coherent components (r_{GP}^{coh}) (Shi et al., 2002). r_{GP}^{non} is computed by integrating over the upper hemisphere the bistatic scattering coefficient ($\sigma_{PP}(\theta, \theta_s, \varphi_s - \varphi)$), which characterizes the scattering of radiations from a direction (θ, φ) to the direction (θ_s, φ_s).

$$r_{GP}^{non} = 1/(4\pi\cos\theta) \int_{hemisph.} (\sigma_{PP}(\theta, \theta_s, \varphi_s - \varphi) + \sigma_{PQ}(\theta, \theta_s, \varphi_s - \varphi))\sin\theta_s d\theta_s d\varphi_s \qquad (4)$$

the subscript P or Q is for polarization and s indicates the direction of the scattered radiation.

r_{GP}^{coh} is written as a function of the Fresnel reflectivity $r^*_{GP}(\theta)$:

$$r_{GP}^{coh}(\theta) = r^*_{GP}(\theta)\exp[-(4\pi S_D\cos\theta/\lambda)^2] \qquad (5)$$

where S_D is the standard deviation of the surface height and λ the wavelength.

This formulation is generally very useful to understand better the physics of scattering effects at the soil surface. The computation of the bistatic scattering coefficients σ_{PP} and σ_{PQ} in Eq. (4) can be obtained from complex modelling approaches such as AIEM (Advanced Integral Equation Model, Chen et al., 2003). For instance, based on this approach, Shi et al. (2002) showed that roughness effects differ strongly at different incidence angles and polarizations. At large incidence angles ($\theta \approx 50°$), as the roughness effects increase (e.g. S_D/λ increases) the emission was found to increase at H polarization. Conversely, at V polarization, the emission was found to decrease, so that the near-black-body emission near the Brewster angle is not reached by rough surfaces, and thus was generally lower than that of flat surfaces.

However, the formulations (4) and (5) are not complete as they do not account for the fine-scale roughness (see the air-to-soil transition model (Schwank & Mätzler, 2006)) and they assumed that only surface scattering effects occur, neglecting the fact that volume scattering effects might strongly affect the soil reflectivity. Also, they are not very tractable for interpreting spaceborne observations: complex theoretical approaches such as the AIEM approach, which are used to compute r_{GP}^{non}, require model inputs describing the spatial variations of the surface height (S_D or the autocorrelation function $\rho(\zeta)$) which cannot easily be related to actual surface characteristics over large SMOS pixels.

To model roughness effects, L-MEB is based on a semi-empirical approach which has been tested against experimental data sets at L-band. The approach was developed initially by Wang and Choudhury (1981) and is based on two best-fit

parameters, H_R and Q_R. The p-polarized soil reflectivity, r_{GP}, is given by:

$$r_{GP}(\theta) = [(1 - Q_R)r^*_{GP}(\theta) + Q_R\ r^*_{GQ}(\theta)]\exp(-H_R\cos^2(\theta)) \qquad (6)$$

The general form of this equation, for the specific case $Q_R = 0$, is similar to the coherent component of soil reflectivity as given in Eq. (5). This general form was gradually modified. After two initial studies considering the $\cos^2(\theta)$ dependence in the exponential term of Eq. (6) (Choudhury et al., 1979; Wang & Choudhury, 1981), Wang et al. (1983) considered in a more detailed study that the $\cos^2(\theta)$ dependence was much too strong. Also, in the classical approach given by Eq. (6), considering that H_R increases with surface roughness effects leads to consider that emissivity increases with roughness at both H and V polarizations, which is in contradiction with theoretical analysis (Mo & Schmugge, 1987; Shi et al., 2002). The H_R parameter should be thus considered as dependent on angle and polarization. Therefore a generalized semi-empirical formulation of roughness effects can be written as:

$$r_{GP}(\theta) = [(1 - Q_{Rp}(\theta))\ r^*_{GP}(\theta) + Q_{Rp}(\theta)\ r^*_{GQ}(\theta)]\exp(-H_{RP}(\theta)\cos^{N_{RP}}(\theta)) \qquad (7)$$

In this generalized formulation, the dependence of Q_R and H_R on θ and polarization is accounted for and the N_{RP} exponent is inserted in the exponential term as in Prigent et al. (2000). Several simplifications can generally be applied to this equation. For instance, Wang et al. (1983) found that the frequency dependence of Q_R was strong and very small values for Q_R were obtained at L-band (for three soil types the best fit values of Q_R were 0, 0.01 and 0.12). This is in agreement with most of the published studies based on a large experimental data set which considered that $Q_R = 0$ (Mo & Schmugge, 1987; Wegmüller & Mätzler, 1999; Wigneron et al., 2001). Note that the value of Q_R was a non-zero parameter at higher frequencies (Njoku & Li, 1999; Pellarin et al., 2006; Shi et al., 2005; Wang et al., 1983).

Setting Q_R equal to zero, we obtain at L-band,

$$r_{GP}(\theta) = r^*_{GP}(\theta)\exp(-H_{RP}(\theta)\cos^{N_{RP}}(\theta)) \qquad (8)$$

As for N_R, Wang et al. (1983) found that $N_R = 0$ was consistent with measurements at three frequencies (1.4, 5 and 10.7 GHz). Mo and Schmugge (1987), Wigneron et al. (2001) also considered that $N_R = 0$ at L-band. An important result was obtained recently by Escorihuela et al. (submitted for publication) in a study based on long term measurements over a relatively smooth soil ($S_D \approx 1$ cm, SMOSREX experiment, De Rosnay et al., 2006a). The authors showed that values of N_R should be given for both polarizations: $N_R \approx 1$ at H polarization and $N_R \approx -1$ at V polarization. Generalization of this result for other roughness conditions should be made.

The dependence of the model roughness parameter $H_{Rp}(\theta)$ on the surface roughness characteristics (S_D, autocorrelation length L_C, etc.) is not well known. Two studies (Mo & Schmugge, 1987; Wigneron et al., 2001) found that the best

geophysical parameters to model H_R were the slope parameter ($m = S_D/L_C$) and the surface soil moisture SM. The dependence of H_R on SM could be explained by an effect of volume scattering: as the soil dries out, emission originates from deeper layers within soil. Possibly, the spatial fluctuations of the dielectric constant within the soil volume are strong during drying out, producing an important "dielectric" roughness effect. Therefore, H_R could be considered as an effective parameter that accounts for (i) "geometric roughness" effects, in relation with spatial variations in the soil surface height, and (ii) "dielectric roughness" effects in relation with the variation of the dielectric constant at the soil surface and within the soil which can be caused by non-uniformities in the soil characteristics. Note that recent results obtained by Escorihuela et al. (submitted for publication) over the SMOSREX bare soil confirmed the general soil moisture dependence of H_R and found that a linear dependence was preferable to the exponential as given by Wigneron et al. (2001).

2.2.2. Soil effective temperature

At L-band, the sampling depth corresponding to the thickness of the soil layer contributing to the microwave soil emission can be large: about 1 m for dry sand (Mätzler, 1998). Therefore, the soil moisture and temperature vertical profiles may have a significant influence on the soil microwave emission. To take this into account, the effective soil temperature T_G contributing to the soil microwave emission can be computed from the radiative transfer theory as (Choudhury et al., 1982):

$$T_G = \int_0^\infty T_S(z)\alpha(z)\exp\left[-\int_0^z \alpha(z')dz'\right]dz \qquad (9)$$

where $T_S(z)$ is the soil temperature at depth z, and the attenuation coefficient $\alpha(z)$ is related to the soil dielectric constant as:

$$\alpha(z) = (4\pi/\lambda) \cdot \varepsilon_G''(z)/2(\varepsilon_G'(z))^{1/2} \qquad (10)$$

where λ is the wavelength of observation, ε_G' and ε_G'' are the real and imaginary part, respectively, of the soil dielectric constant.

Based on this formulation and experimental data, Choudhury et al. (1982) developed a simple parameterization of the effective soil temperature T_G:

$$T_G = T_{\text{soil\_depth}} + C_t(T_{\text{soil\_surf}} - T_{\text{soil\_depth}}) \qquad (11)$$

where $T_{\text{soil\_depth}}$ is the deep soil temperature (approximately at 50 or 100 cm); $T_{\text{soil\_surf}}$ is the surface temperature (approximately corresponding to a depth interval of 0–5 cm).

Choudhury et al. (1982) calibrated constant values of the C_t parameter for several frequency bands and C_t was found to be equal to 0.246 at L-band. In reality, the dependence of C_t on soil moisture should also be taken into account. For instance, if the soil is very dry, soil layers at depth (deeper than 1 meter for dry sand) contribute significantly to the soil emission, and the value of C_t is lower than 0.5. Conversely, if the soil is very wet, the soil emission originates mainly from layers at the soil surface and $C_t \approx 1$. Taking this into account, Wigneron et al. (2001) introduced a slight refinement in Eq. (11). They considered that

$T_{\text{soil\_depth}}$ is the soil temperature at 50 cm and they parameterized C_t as a function of the surface soil moisture according to:

$$C_t = (S_M/w_0)^{bw0} \qquad (12)$$

where S_M is the 0–3 cm surface soil moisture, which corresponds well to the effective SM value contributing to soil emission at L-band (Raju et al., 1995), w_0 and b_{w0} are semi-empirical parameters depending on the specific soil characteristics (mainly soil texture).

Holmes et al. (2006) developed a similar parameterization of C_t based on the dielectric constant ε_G which provided slightly improved results but is a bit more complex as it requires the additional use of a model simulating ε_G. L-MEB is based on the earlier and simpler Eq. (12) which was tested over several sites and whose long term suitability was shown by De Rosnay et al. (2006b) at the seasonal to inter-annual temporal scales. The value of w_0 was found to be close to 0.3 m³/m³ over two bare soil sites: INRA Avignon (Wigneron et al., 2001) and SMOSREX (De Rosnay et al., 2006b). The value of b_{w0} was close to 0.3 m³/m³ over the INRA Avignon site and close to 0.65 m³/m³ over the SMOSREX site. The modelling of w_0 and b_{w0} as a function of soil texture is currently in progress. At present the values $w_0 = 0.3$ m³/m³ and $b_{w0} = 0.3$ are used as default values in L-MEB.

Note that the simple formulations (9) (10) (11) and (12) neglect multiple scattering effects within the soil layer. However, accounting for these effects by numerical electromagnetic models would require a very detailed description of the soil heterogeneities which can be only obtained over very small soil samples. So, currently, we think that even though Eqs. (9), (10), (11) are based on a relatively simplified description of the soil volume scattering effects, they are simple and accurate enough to be used in L-MEB for retrievals at relatively large spatial scales.

2.2.3. Soil permittivity

Two main models have been developed for the low frequency range (1–20 GHz) to relate the soil permittivity to soil parameters such as soil moisture, soil salinity, bulk density, % of sand and clay (Dobson et al., 1985; Wang & Schmugge, 1980). In L-MEB, the model of Dobson et al. (1985) was used to compute ε_S in the general case, except for dry sandy soils (where a simplified approach proposed by Mätzler (1998) was used).

Soil freezing also affects ε_G considerably. Measurements of soil dielectric constant at L-band have been obtained by Hallikainen et al. (1984, 1985) in wet, frozen and unfrozen conditions. According to these observations, the real part of ε_G (ε_G') is close to 5 for frozen soils. This value is relatively independent of soil texture, temperature and frequency. For very low temperatures (close to −50 °C) and for specific soil textures, ε_G' may decrease down to 4. The imaginary part of ε_G (ε_G'') of a frozen soil was found to be lower than 1 for most soil types. The values of ε_G'' depend significantly on temperature. For very low soil temperatures (lower than −50 °C), ε_G'' can be close to zero. However, for temperatures between −0.5 and −10 °C, ε_G'' is close to 0.5 for most soil types. Similar

conclusions were obtained by Mätzler (1993) who noted that for frozen soil (a sandy loam) the value of ε_G' seemed to decrease from 5 at -1 °C to about 4 at -6 °C. As no detailed model is available to parameterize accurately the possible effect of water inclusion in frozen soil, the permittivity of frozen soil (ε_{GF}) was set equal to a constant:

$$\varepsilon_{GF} = 5 + 0.5i \tag{13}$$

A simple evaluation of this formula was done by Wigneron et al. (2006a) and showed that, if ε_G' is set equal to 5, the surface emissivity at both polarizations is almost insensitive to variations of ε_G'' in the 0.01–1 range (however the penetration depth remains directly related to ε_G''). The sensitivity of the emissivity to the real part of ε_G is much stronger.

2.3. Vegetation modelling

2.3.1. General

When a vegetation layer is present over the soil surface, it attenuates soil emission and adds its own contribution to the emitted radiation. At low frequencies, these effects can be well approximated by a simple Radiative Transfer (R. T.) model, hereafter referred to as the τ–ω model. This model is based on two parameters, the optical depth τ_p and the single scattering albedo ω_P, which are used to parameterize, respectively, the vegetation attenuation properties and the scattering effects within the canopy layer (Mo et al., 1982). This model is a zero-order solution of the radiative transfer (R.T.) equations as it assumes that the scattering phase matrix term can be neglected (Ulaby et al., 1981-1986; Mätzler et al., 2006). The τ–ω model has usually been found to be an accurate approach to model the L-band emission from a vegetation canopy in numerous studies (Brunfeldt & Ulaby, 1984; Hornbuckle et al., 2003; Jackson & Schmugge, 1991; Kerr & Njoku, 1990; Mo et al., 1982; Pampaloni & Paloscia, 1986; Wigneron et al., 1995) and it is also a tractable tool for inversion processes (Van de Griend & Owe, 1993; Wigneron et al., 1995, 2000, 2003).

Note that in theory, a coherent model that considers scattered fields, and not only scattered intensity as in R.T. models, would be required. Phase interference effects could be important at low frequencies (L- and P-bands) where the wavelength is of the order or greater than the typical size of the vegetation elements. These effects occur at the scale of plant components and at the scale of plant distribution (e.g. row structure). Thus, the vegetation R. T. model parameters which are calibrated from experimental measurements implicitly account for these effects and should thus be considered as effective values resulting from complex coherent scattering mechanisms (Mätzler et al., 2006). However, these coherent effects are particularly important for active systems and when the antenna footprint is very narrow (Stiles et al., 2000). It is likely they are lower for passive systems measuring the surface emissivity, which is related to the integral of the bistatic scattering pattern. This will be partially confirmed by the general consistency of the results obtained in Section 4, from observations for varying azimuthal viewing configurations relatively to the vegetation rows.

Using the τ–ω model, global emission from the two layer medium (soil and vegetation) is for each polarisation 'P' the sum of three terms: (1) the direct vegetation emission, (2) the vegetation emission reflected by the soil and attenuated by the canopy layer and (3) soil emission attenuated by the canopy:

$$T_{BP} = (1-\omega_P)(1-\gamma_P)(1+\gamma_P \, r_{GP})T_C + (1-r_{GP})\gamma_P \, T_G \tag{14}$$

where T_G and T_C are the effective soil and vegetation temperatures, r_{GP} is the soil reflectivity, γ_P the vegetation attenuation factor.

This last term can be computed from the optical depth τ_P as:

$$\gamma_P = \exp(-\tau_P/\cos\theta) \tag{15}$$

As presented in the following, τ_P is expressed as a function of the overall optical depth at nadir τ_{NAD} (at $\theta = 0°$).

In addition to soil reflectivity (r_{GP}), three main effects can be distinguished in Eq. (14): those of temperature (through both T_G and T_C terms), vegetation scattering (ω_P) and attenuation (τ_P). Computation and calibration of these three terms are discussed below.

- Temperature: in most retrieval studies, it is assumed that effective soil (T_G) and vegetation (T_C) temperatures are approximately equal to a single value $T_{GC} \approx T_C \approx T_G$. In particular, the effects of temperature gradients within the vegetation canopy are not accounted for. With an overpass around dawn these gradients should be minimised and T_C can be expected to be close to the air temperature, while T_G can be estimated from atmospheric models outputs (Hornbuckle & England, 2005). In L-MEB, an estimate of an effective composite temperature T_{GC} (including both soil and vegetation media) was proposed:

$$T_{GC} = A_t T_C + (1-A_t)T_G \tag{16}$$

with

$$A_t = B_t(1-\exp(-\tau_{NAD})) \tag{17}$$

$$A_t \leq 1 \tag{18}$$

where the parameters A_t and B_t account for the effect of the vegetation structure and are assumed to depend on the canopy type (when computing A_t, values exceeding unity are set to unity). The rationale of these equations is that as optical depth τ_{NAD} increases, both (i) attenuation of soil emission and (ii) vegetation emission increase, making the effective temperature T_{GC} closer to the vegetation effective temperature. Conversely, for bare soil conditions (ie for $\tau_{NAD}=0$), T_{GC} is equal to T_G. The coefficient B_t is a function of the vegetation structure which is determined mainly by the canopy type. When θ increases, T_{GC} becomes closer to the vegetation temperature as attenuation by the vegetation increases due to the $1/\cos\theta$ dependence in Eq. (15). However, so as to simplify the modelling of T_{GC}, the effects of this dependence were neglected.

An estimate of the default value of B_t, $B_t=1.7$, was numerically derived by applying Eqs. (16), (17) to a synthetic T_B data set simulated with the τ–ω model for a large range of

values of optical depth, soil and vegetation temperatures and incidence angles (Kerr et al., 2006). To evaluate the interest of this formulation, let us consider a typical case study: a mature crop ($\tau_{\text{NAD}} \approx 0.3$) with a 6 K difference between the soil and vegetation effective temperatures. Using directly T_C or T_G in the algorithm instead of the composite temperature T_{GC} given by Eqs. (16) and (17), may lead to wrongly estimate T_{GC} by about ± 3 K (and the retrieved SM by about 0.01 m^3/m^3). Therefore, the impact of using this composite formulation in the algorithm is relatively low but it is not negligible. Future studies will evaluate this simplified formulation of T_{GC} more in depth from experimental data sets.

- Scattering effects: at L-band, the value of the single scattering albedo ω_P is generally found in the literature to be low. For specific crop types (such as corn), ω_P can reach a value close to 0.1, but for most of low vegetation types, ω_P is lower than 0.05 (Wigneron et al., 2004). As the dependence of ω_P on θ has not been clearly demonstrated to date in the literature, this dependence was neglected in L-MEB and the value of ω_P is tabulated as a function of the vegetation type. Similarly, it is likely that the dependence of ω_P on polarization is low for most of low vegetation canopies.

- Optical depth: several studies have found that τ_P can be related linearly to the total vegetation water content V_{WC} (kg/m^2) using the so-called b_P parameter ($\tau_P = b_P V_{\text{WC}}$, Jackson & Schmugge, 1991; Van de Griend & Wigneron, 2004). At 1.4 GHz a value of $b_P = 0.12 \pm 0.03$ was found to be representative of most agricultural crops. In L-MEB a different modelling approach was used, accounting for several recent results. The main effects included are given below:

  – as it is difficult to provide estimates of V_{WC} at global scale, the contribution of the standing vegetation to τ_P was parameterized as a function of the Leaf Area Index (LAI).
  – some studies have investigated in more detail the effects of the vegetation structure which may affect the dependence of τ_P on polarization and incidence angle (Hornbuckle et al., 2003; Schwank et al., 2005; Ulaby & Wilson, 1985; Wigneron et al., 1995, 2004). As the SMOS algorithm is based on polarized and multi-angular measurements, it was important to account for this dependence.
  – several studies have shown that the effect of litter is significant (Jackson & Schmugge, 1991; Saleh et al., 2006a; Schmugge et al., 1988). Litter can be present in most vegetation canopies, which are not (or rarely) ploughed: prairies or non-agricultural canopies, natural covers, forests, etc. For instance, while a value of b_P close to 0.15 was generally found over crops, very high values of the b_P parameter ($b_P \approx 0.4$) have been obtained over natural vegetation covers such as prairies (Jackson & Schmugge, 1991; Wigneron et al., 2004). Such high values of b_P could probably be related to the attenuation effects of litter that were accounted for implicitly by the value found for b_P.
  – recent results have shown that the effects of rainfall interception by the vegetation canopy may be very significant: optical depth τ_P may increase by a factor of two or three during and after rainfall, for instance over a fallow (Saleh et al., 2006a).

In order to account for these different effects in L-MEB, we considered the total optical depth τ_P to be a combination of multiple component optical depths:

$$\tau_P = \tau_{\text{SP}} + \tau_L + \tau_{\text{IP}} \tag{19}$$

where τ_{SP} is the optical depth of the standing vegetation cover, τ_L is the optical depth of all the vegetation materials laying at the bottom of the canopy (including litter mainly), and τ_{IP} is used to parameterize the increase in optical depth due to intercepted water by the standing vegetation canopy. The computation of these three terms is given below.

2.3.2. Optical depth of the standing vegetation

τ_{SP} is the optical depth of the standing vegetation cover, including both green and senescent vegetation materials. Even though τ_{SP} was usually found to be closely related to V_{WC}, τ_{SP} was parameterized as a function of the Leaf Area Index (LAI) in L-MEB. There are two main reasons for this: (i) it is much easier to construct global maps of LAI from spaceborne remote sensing observations in the optical domain or from SVAT modelling (Wigneron et al., 2002) than construct maps of V_{WC} directly; (ii) recent studies have found good correlation between τ_{SP} and LAI (Saleh et al., 2006a). Jackson et al. (2004) investigated the link between V_{WC} and Normalized Vegetation Indices (NDVI or NDWI) computed from optical spaceborne sensors and they obtained a good prediction of V_{WC} from NDWI over corn and soybeans fields. The relationship between V_{WC} and LAI is investigated in the present study for several crops as it is likely that the parameterization of τ_{SP} from LAI, rather than from V_{WC}, will be efficient as long as the vegetation is green. But it might be less accurate during the senescent phase during which the microwave optical depth of dead or senescent vegetation materials might be underestimated from low LAI values. However, it is likely that very accurate estimations of LAI are not required in the SMOS algorithm. Uncertainties on the estimations of optical depth have a large impact on the SM retrievals, when only SM is retrieved. However, in the Level 2 algorithm, estimates of optical depth at nadir (τ_{NAD}) are obtained directly from retrievals based on the multi-angular SMOS observations (Wigneron et al., 2000). Estimates of τ_{NAD} computed from LAI, are used only to initialize the value of τ_{NAD} in the retrievals. It is thus expected that the uncertainties on the LAI values have a relatively low impact on the SM retrievals.

The effect of vegetation structure on τ_{SP} was found to be significant in several studies. Wigneron et al. (1995) proposed a simple formulation using a polarization correction factor C_{pol} to parameterize the effect of a dominant vertical vegetation structure on the optical depth for cereal crops:

$$\tau_{\text{SH}}(\theta) = \tau_{\text{S\_NAD}} = \text{constant} \tag{20}$$

$$\tau_{\text{SV}}(\theta) = \tau_{\text{S\_NAD}}[\cos^2\theta + C_{\text{pol}}\sin^2\theta] \tag{21}$$

where $\tau_{\text{S\_NAD}}$ is the value of τ_{SP} at nadir.

Within each pixel, the contributions of the dominant vegetation types are summed, at a sub-grid scale, to compute

the microwave emission corresponding to the nominal class (soil and low vegetation covers). By summing these contributions over a large variety of vegetation types at the relatively coarse pixel scale, specific effects of the vegetation structure are mixed, so that the dependence of the equivalent τ_{SP} and ω_P parameters on polarization and incidence angle might be low over most pixels (Owe et al., 2001). However, the possibility of accounting for this dependence must be kept in the algorithm at this stage. For instance, in regions including many large cereal fields, specific effects due to the vegetation structure might have an impact on the large scale SMOS pixel emission. Thus a generalization of Eqs. (20), and (21) was developed in L-MEB. We chose to express $\tau_{SV}(\theta)$ and $\tau_{SH}(\theta)$ as a function of only one variable, namely, τ_{S_NAD}, which is estimated as a function of LAI. The modelling of $\tau_{SP}(\theta)$ was thus written in three equations as follows:

$$\tau_{S\_NAD} = b'_S \cdot LAI + b''_S \tag{22}$$

where the b'_S and b''_S parameters depend mainly on the vegetation structure. $\tau_{SV}(\theta)$ and $\tau_{SH}(\theta)$ were expressed as function of τ_{S_NAD} according to:

$$\tau_{SH}(\theta) = \tau_{S\_NAD}(\sin^2(\theta) \cdot tt_H + \cos^2(\theta)) \tag{23}$$

$$\tau_{SV}(\theta) = \tau_{S\_NAD}(\sin^2(\theta) \cdot tt_V + \cos^2(\theta)) \tag{24}$$

where the tt_V and tt_H parameters allow accounting for the dependence of τ_{SP} on incidence angle. These two equations are a generalization of the equations based on the C_{pol} factor which correspond to the particular case: $tt_H = 1$ and $tt_V = C_{pol}(C_{pol} > 1$ for a vertical structure).

Formulations (23) and (24) are very simple even though they allow parameterizing $\tau_{SP}(\theta)$ for a variety of land cover configurations. A value of $tt_P > 1$ or $tt_P < 1$ will correspond, respectively, to an increasing or decreasing trend of τ_{SP} as a function of θ. The particular case, $tt_H = tt_V = 1$, will correspond to the "isotropic" case where τ_{SP} is assumed to be independent of both polarizations and incidence angle: $\tau_{SH}(\theta) = \tau_{SV}(\theta) = \tau_{S\_NAD}$.

2.3.3. Litter and interception effects

As noted above, the effects of litter and interception on the vegetation microwave emissivity have been investigated and found to be very significant over prairie grassland and fallow (Saleh et al., 2006a,b; Schmugge et al., 1988). In Eq. (19), τ_L is the optical depth of a mixed and dense layer overlying the ground surface and including mainly dead vegetation. As this layer is very dense in terms of volumetric fraction f_V (m^3/m^3) (i.e. volume of vegetation material (m^3) per volume of the vegetation layer (m^3)), its attenuation properties might well be very different from those of a standing vegetation cover. Also, this layer includes mainly dead or senescent vegetation materials which have a very high retention capacity for intercepted water (Putuhena and Cordery, 1996). Rainfall intercepted by this layer evaporates generally at a much lower rate (on a daily basis) than that intercepted by the standing vegetation, which evaporates on an hourly basis. Thus, the

water content of this layer is strongly dependent on the rainfall events and is generally closely related to the soil moisture content. As the optical depth of the vegetation material is generally related to its total water content, the following equation was used in L-MEB for litter:

$$\tau_L = c_L L_{WC} \tag{25}$$

where c_L is a coefficient characterizing the attenuation properties of litter and L_{WC} is the amount of water included in this layer (kg/m^2).

As litter probably has isotropic attenuation properties, c_L was assumed to be polarization independent. The coefficient c_L will depend mainly on the canopy type which will determine the characteristics of the litter (density, material type, etc.). Recent results obtained from microwave measurements acquired over a fallow land during the SMOSREX experiment confirmed Eq. (25) and the estimated value of c_L was $c_L = 0.24$ (Saleh et al., 2006a). This value was at least twice that of b_P, confirming possibly higher attenuation properties for litter than for the standing canopy. L_{WC} was computed as a function of the litter moisture content (Mg_L kg/kg), which is the ratio of the litter water content (kg) to the total litter weight (kg), and of the litter dry biomass (B_S_L, kg/m^2) as follows:

$$L_{WC} = [Mg\_L/(1-Mg\_L)]B_S\_L \tag{26}$$

In L-MEB, the dry biomass of litter (B_S_L) is estimated as a function of the canopy type. Based on experimental results obtained over a pine forest (Grant et al., 2007), it is assumed that Mg_L can be related empirically to the soil moisture content (S_M) following an approximate linear relationship:

$$Mg\_L = a\_L \cdot S_M + b\_L \atop \text{with } 0 \le MgL \le 0.8 \tag{27}$$

It is assumed that the a_L and b_L parameters, which depend on the litter characteristics, can be estimated as a function of the canopy type.

In Eq. (19), τ_{IP} is the optical depth which parameterizes the effect of intercepted water by the standing vegetation canopy, because of rainfall or dew events (effects of interception by litter were included in τ_L). For a moderate amount of intercepted water or dew events (less than 1.5 mm intercepted water), the L-band measurements still remained very sensitive to soil moisture (Wigneron et al., 1996). However, recent results showed that the effects of intercepted water could be significant (Hornbuckle et al., in press; Saleh et al., 2006a,b). Over a fallow (Saleh et al., 2006a,b), the optical depth of the vegetation was found to increase by a factor of two or more after rainfall events. The water can be intercepted by (i) the green vegetation material (the water is mainly on the surface of the vegetation elements) (ii) senescent or dead standing vegetation elements (the water is mainly adsorbed by the dead vegetation tissue) (iii) or by the litter. Over some natural vegetation covers, the fraction of dead or senescent vegetation elements within the litter or the standing vegetation may be significant.

An attempt to parameterize τ_{IP} would require unreliable estimations of the interception reservoir (mm) and of the fraction of intercepted water (Noilhan & Planton, 1989), which depends on the intensity of the rainfall events and size of evaporation fluxes. Rather than attempting to model the interception intensity, an index flagging events during which interception effects are very significant (and during which it is very likely that soil moisture cannot be retrieved) was used in L-MEB. Results by Saleh et al. (2006a,b) showed that one of the best indices that can be used to flag interception at local scale is the polarization ratio $P_R = (T_{BV} - T_{BH})/(T_{BV} + T_{BH})$ at large incidence angles ($\theta \geq 40°$). P_R values lower than a given threshold (P_{RI}) will correspond to a high probability of significant interception events. In L-MEB it is assumed that this threshold can be parameterized as a function of the vegetation type. However, before more detailed results will be available on that parameterization, the default value of the threshold P_{RI} ($P_{RI} = 0.02$ at $\theta = 50°$) was used, computed by Saleh et al. (2006a) over a fallow site. Note that, from the microwave observations only, it would be very difficult to separate between the increasing effects on the vegetation optical depth due to intercepted water either (i) in the standing vegetation or (ii) in the litter as done in (19). Therefore, the flag which was suggested should be considered as an interception index flagging for significant effects due to total interception within both litter and standing vegetation.

2.4. Forests

As mentioned in Introduction, the case of forests will be the subject of another paper. Over this canopy type, litter was also accounted for and the ω and τ_{NAD} parameters were fitted over T_B data bases simulated by a discrete model under various assumptions (Della Vecchia et al., in press). The main conclusions of this study are summarized below (the subscript "F" will refer to forest canopies):

- τ_{F_NAD} was assumed to be constant with respect to polarization and angle. This was a result of the variability in orientation of branches and leaves in forest canopies.
- τ_{F_NAD} was considered as a "static" parameter which did not change in time. τ_{F_NAD} was related to the maximum value of LAI over the year, which is in relation with branch volume, and which may be assumed to be constant during SMOS life time (about four years). This is a result of the dominance of branch effects with respect to leaf effects at L-band (in agreement with previous results of Ferrazzoli et al., 2002).
- ω_F was considered as constant (i.e. independent on angle, polarization and time). However, contrary to low vegetation, the value of ω_F is not negligible, but it is of the order of 0.1.

3. Materials and methods

The implementation of L-MEB in the SMOS Level-2 Soil Moisture inversion algorithm requires the calibration of the soil and vegetation model parameters. In order to illustrate this, and the use of L-MEB in inversion studies, retrievals were applied to several experimental data sets. This section presents the data sets and the inversion method which were used here. These data sets come from observations over agricultural fields which are regularly ploughed and where there is no litter layer. Tests of L-MEB over vegetation cover types including a litter are investigated in another companion study for low natural vegetation cover and grassland prairies (Saleh et al., submitted for publication). As litter and interception are not considered in the present study, τ_L and τ_I are equal to zero in Eq. (19).

3.1. Data sets

Experimental multi-angular data sets acquired over a variety of crops were used in this study. PORTOS-91 was obtained over soybean (Wigneron et al., 1993a,b), PORTOS-93 over wheat (Wigneron et al., 1995), EMIRAD-2001 over corn (Pardé et al., 2004), REBEX over corn (Hornbuckle et al., 2003) and BARC over corn and soybean (Wang et al., 1982). A detailed description of these experiments was given in the above-cited references. Only the main features of these experimental data sets will be presented briefly below.

The PORTOS −91 and −93 campaigns were conducted in 1991 and 1993 on a plot located at the INRA (Institut National de la Recherche Agronomique) Avignon test site. During both campaigns, the brightness temperature was measured by the dual-polarization multifrequency PORTOS radiometer. During both PORTOS −91 and −93, the sensor was hung from a 20-m crane boom, and observations were carried out at different incidence angles (from 0° to 60°). Note that for PORTOS −93, two periods were considered: the whole vegetation cycle (DoY 110–186) and the DoY 110–160 period before irrigation. The irrigation, applied after the wheat had become senescent, significantly altered the vegetation structure.

The EMIRAD-2001 data set was obtained over a corn field (about 80×120-m) at the same Avignon test site using the L-band EMIRAD instrument designed by the Technical University of Denmark (TUD); this was also hung from a 20-m crane boom. The measurements were made for an azimuthal viewing configuration either parallel or orthogonal to the vegetation rows (referred to as the // and ⊥ azimuthal configurations) during a three-month period spanning the whole green vegetation stage in 2001.

The REBEX (Radiobrightness and Energy Balance Experiments) experiments were conducted during the spring, summer, and autumn of 2001 over an 800×400 m corn field in southeastern Michigan. Measurements were mainly carried out at five times: over bare soil, during vegetation growth (twice), at maximum biomass, and during senescence. Two radiometers, oriented to record H-pol and V-pol 1.4-GHz brightness, were mounted on the hydraulic arm of a truck. Brightness temperatures were measured at incidence angles of 15°, 35°, and 55° shortly after dawn when soil and canopy temperatures were nearly uniform. Measurements were acquired for several azimuthal angles (ϕ) with respect to row direction: only data for $\phi = 60°$ will be analysed in this study.

The *BARC* data set was acquired in 1981 in Beltsville (Maryland, USA), over several crops and bare soil plots. The

Table 2
Soil characteristics over the different experimental sites

Data set	Density (g/cm^3)	Sand %	Clay %
PORTOS-91 and-93	1.29	11	27
EMIRAD-2001	1.28	13.2	32.8
REBEX	1.1	16	29
BARC	1.2	67	15

Note: Salinity (‰) was set to 0.65 for all data sets.

L-band radiometer was mounted on a mobile tower and measurements were made at incidence angles (θ) varying from 10 to 70° with a 10° step for both H and V polarizations. Measurements over corn and soybean for the // and ⊥ azimuthal viewing configurations were analyzed in this study.

During all these experiments, soil and vegetation measurements were carried out concurrently with the radiometric measurements. The values of the soil texture parameters and the bulk soil density are given in Table 2 for all fields. Profiles of soil moisture and temperature were measured at the time of the T_B observations. Measurements of dry and wet biomass and LAI (except for BARC) were also carried out regularly during all experiments. The time variations in the amount of water in the vegetation canopy (V_{WC}, kg/m^2) are illustrated in Fig. 1 over all fields. In this figure, each symbol corresponds to a date of radiometric measurements. No cross-sensor calibration of the radiometric data could be made for these different experiments which were carried out over the last twenty years. The accuracy of the PORTOS instrument (which is estimated to be in the 3–5 K range) was probably slightly lower than that of the other instruments: about 2–3 K for the EMIRAD-2001, REBEX and BARC data sets. For all these experiments the agricultural soils were relatively smooth, except for the two corn fields of the REBEX and BARC: the average standard deviation of height σ_{SOIL} was about 2.5 cm over corn (Hornbuckle et al., 2003) and it was generally less than 1 cm for the other experiments.

3.2. Inversion method

The retrievals were based on the inversion of the L-MEB model. The surface parameters were retrieved by minimizing a cost function (CF) using a generalized least-squares iterative algorithm modified to account for *a priori* information available on the model input parameters. This *a priori* information consisted of (i) the initial value of the parameters (S_M, τ_{NAD}, T_{GC},...), and (ii) the uncertainty ($\sigma(S_M)$, $\sigma(\tau_{NAD})$, $\sigma(T_{GC})$...) associated with these estimates. The cost function was computed as (Pardé et al., 2004):

$$CF = \frac{\Sigma(T_{Bmes} - T_B{}^*)^2}{\sigma(T_B)^2} + \sum_i \frac{\Sigma(P_i^{ini} - P_i{}^*)^2}{\sigma(P_i)^2} \qquad (28)$$

where the sum of the difference between measured (T_{Bmes}) and simulated ($T_B{}^*$) brightness temperature was computed using both polarizations and all available incidence angles ($\theta \leq 55°$ were considered in this study); $\sigma(T_B)$ is the standard deviation

associated with the brightness temperature measurements; $P_i{}^*$ ($i=1,... N$) is the value of the retrieved parameter (S_M, τ_{NAD}, T_{GC}, H_R, ω_H, tt$_H$, tt$_V$, etc.); P_i^{ini} ($i=1, ... N$) is the initial value of each parameter in the retrieval process and corresponds to an *a priori* estimate of the parameter P_i; $\sigma(P_i)$ is the standard deviation associated with this estimate. The second term in the cost function allows to take into account *a priori* information on the value of the retrieved parameters: if they are known *a priori*, the average value of the retrieved parameter and the uncertainty associated to this average (considered as a Gaussian distributed parameter) can be introduced in Eq. (28) to constrain the retrievals. All the uncertainties on the T_B observations and the surface parameters are considered as random and independent in both the first and second terms of Eq. (8). In the first term of Eq. (8), the multi-angular and dual polarization T_B observations can be considered as independent, considering the technical specifications in the design of the antenna and the time delay between the multi-angular observations. In the second term of Eq. (8), the uncertainties associated with the initial value of each parameter can also be considered as independent, as derived from independent approaches (atmospheric model outputs, maps of the canopy types derived from optical sensors, etc.).

Depending on the constraints and initial values used, a large number of retrieval configurations can be tested. These configurations have been tested in detail in the study of Pardé et al. (2004) and will not be repeated here. In the present study we selected a single retrieval configuration for all data sets which consisted in the retrieval of three parameters (S_M, τ_{NAD}, H_R). This configuration, referred to as the '3-P' approach in the following, is simple and performed well over all experimental data sets. An arbitrary very high value was selected for $\sigma(S_M)$ so that S_M can be considered as a free parameter ($\sigma(S_M) = 0.3$ m^3/m^3). The optical thickness was initialized using the value which was retrieved ($\tau_{NAD}{}^*$) at the previous
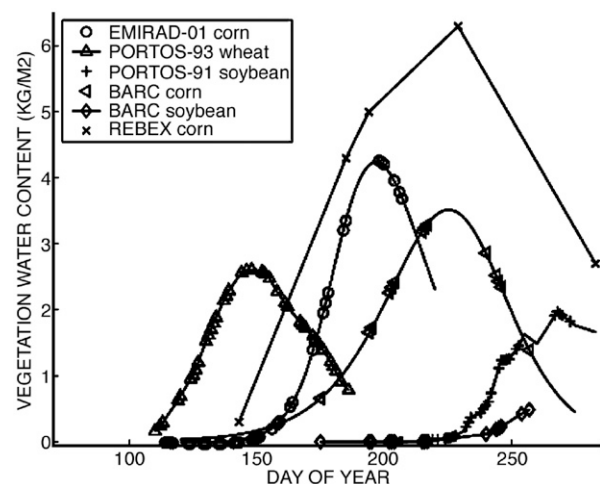
Fig. 1. Time variations in the vegetation water content (V_{WC}, kg/m^2) over the different fields of crop. Each symbol corresponds to a date of radiometric measurement. For EMIRAD-01, PORTOS-91 and -93 smoothed data, obtained by fitting a logistic-type function to the actual V_{WC} measurements (as in Saleh et al., 2006a), are shown.

Table 3
Initial configuration of the retrieval process ('3-P' approach)

Parameter (P_i)	Initial value (P_i^{ini})	Standard deviation $(\sigma(P_i))$
Soil moisture, S_M	0.05 m³/m³	0.3 m³/m³
Optical thickness at nadir, τ_{NAD}	$\tau_{NAD} = \tau_{NAD}*(t-1)^1$ at date $t=0$: $\tau_{NAD}=0$	0.05
Effective ground— canopy temperature, T_{GC} (K)	Computed from (16)–(17)	0.1 K (fixed parameter)
Roughness parameter, H_R	Calibrated crop dependent value (given in Table 4)	0.1
Measured T_B		$\sigma(T_B)=2$ K, except: $\sigma(T_B)=3$ K for PORTOS

[1] $t=0$ correspond to the first date of T_B measurements in each data set and $\tau_{NAD}*(t-1)$ is the retrieved value of τ_{NAD} at the date $t-1$ preceding date t.

measurement date ($\tau_{NAD}^{\text{ini}}(t) = \tau_{NAD}*(t-1)$). The initialization for the first date of the data set ($t=0$) was arbitrary made using $\tau_{NAD}^{\text{ini}}(t=0)=0$. Eq. (16) was used to compute an estimate of the effective composite temperature T_{GC}. A summary of these initial values and constraints is given in Table 3. The values of $\sigma(P_i)$ in Table 3 should not generally be considered as estimates of the actual uncertainty on the parameter value P_i. These values should be considered as constraints in the retrievals that were optimized to produce best retrieval results over all data sets. For instance 0.1 K should not be seen as an uncertainty on the temperature estimates but as a very strong constraint so that the effective temperature T_{GC} was not retrieved but could be considered as a fixed parameter.

For each crop, the model parameters (namely H_R, N_{RV} and N_{RH} for soil; tt_H, tt_V, ω_H and ω_V for vegetation (litter was not

considered in this study)) were calibrated. This calibration was based on several criteria evaluating the quality of the retrievals:

- minimum Root Mean Square Error (RMSE) error and bias between measured and retrieved soil moisture.
- minimum value of the average RMSE between the simulated and measured T_B data.
- minimum value of the intercept and maximum value of the squared correlation coefficient (R^2) in the relation between retrieved optical depth (τ_{NAD}) and vegetation water content (V_{WC}). This criteria is based on the assumption, investigated in several studies (Jackson & Schmugge, 1991, Van de Griend & Wigneron, 2004), that τ_{NAD} and V_{WC} are proportional.

4. Retrieval results

The '3-P' approach, in which the three parameters, soil moisture (S_M), optical depth at nadir (τ_{NAD}) and the soil roughness parameter (H_R) were retrieved simultaneously, was tested against all data sets. The model parameters S_M, τ_{NAD} and T_{GC} were initialized as given in Table 3. The other soil and vegetation model parameters were calibrated as defined in the previous section. They are given in Table 4 for each crop. The RMSE between measured and retrieved S_M is also included in this Table. In order to illustrate all these different results, a comparison between measured and retrieved parameters is given for the PORTOS-91 campaign for soil moisture (Fig. 2) and for vegetation water content and LAI (Fig. 3). Similar plots, not shown here, were obtained for the other field experiments (Wigneron et al., in press). The results of the parameter calibration, given in Table 4, are summarized in the following.

As for soil parameters, the calibrated value of H_R was consistent with the ground estimation of soil roughness: the value of H_R was found to be significantly higher for the two corn fields of the US experiments ($H_R \approx 0.5$ for REBEX and BARC) than for the other experiments where the soil roughness conditions were much smoother ($H_R \approx 0.1$). The retrieved value

Table 4
Calibrated model parameters and RMSE between measured and retrieved SM from the '3-P' approach

	H_R	N_{RV}	N_{RH}	tt_H	tt_V	ω_H	ω_V	Number of observation dates	RMSE on S_M (m³/m³)
PORTOS-91, soybean	0.1	0	0	1	2	0	0	32	0.044
PORTOS-93, wheat	0.1	0	0	1	8	0	0		
All_the_data								45	0.061
Data for DOY<161								30	0.042
EMIRAD 2001, corn	0.1	0	0	2	1	0.05	0.05		
⊥ configuration								33	0.042
// configuration								30	0.044
REBEX, corn	0.7	−1	0.5	2	1	0.05	0.05	5	0.025
BARC, soybean									
⊥ configuration	0.2	−1	0	1	1	0	0	11	0.029
// configuration								11	0.053
BARC, corn	0.6	−1	0.5	2	1	0.05	0.05		
⊥ configuration								14	0.035
// configuration								14	0.023

Fig. 2. PORTOS-91: comparison between retrieved and measured soil moisture (m³/m³) using the '3-P' approach.
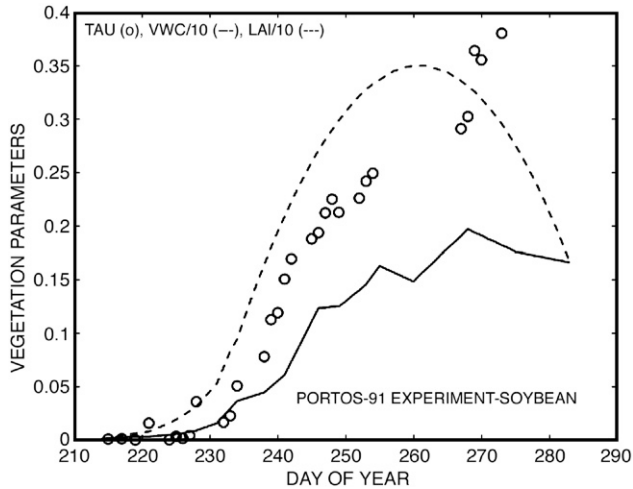
Fig. 3. PORTOS-91: comparison between the time variations of retrieved τ_{NAD} and measured V_{WC} (kg/m^2) and LAI (m^2/m^2).

Table 5
Slope, intercept and squared correlation coefficient (R^2) of the linear regression between retrieved τ_{NAD} vs V_{WC} and retrieved τ_{NAD} vs LAI

Data sets	τ_{NAD} (V_{WC}) relationship			τ_{NAD} (LAI) relationship		
	slope	intercept	R^2	slope : b$'_S$	intercept: b$''_S$	R^2
PORTOS-91, soybean	0.174	0.00	0.96	0.090	−0.020	0.88
PORTOS-93, wheat	0.073	−0.009	0.80	0.017	0.061	0.24
DOY<161[1]	0.077	−0.020	0.89	0.034	−0.010	0.52
EMIRAD-2001, Corn						
⊥ configuration	0.050	0.016	0.82	0.047	0.00	0.80
// configuration	0.046	0.016	0.87	0.039	0.010	0.82
REBEX, Corn	0.044	−0.019	0.92	0.055	−0.018	0.89
BARC[2]				−	−	−
Soybean ⊥	0.207	0.021	0.84			
Soybean //	0.147	0.034	0.67	−	−	−
Corn ⊥	0.060	0.024	0.54	−	−	−
Corn //	0.079	0.005	0.77	−	−	−

[1] After DoY 160, intense irrigations were applied over a senescent canopy and altered the vegetation structure.
[2] LAI was not available in the BARC data set.

of N_{RH} was close to zero generally (N_{RH} varied between 0 and 0.5). The value of N_{RV} was different for the US and INRA data sets: N_{RV} was close to −1 for the REBEX and BARC while it was close to zero for the INRA data sets. The value of $N_{RV}=−1$ is consistent with results obtained by Escorihuela et al. (submitted for publication) from the analysis of the long term SMOSREX data set over a bare soil.

As for the vegetation parameters, very consistent results were obtained since the same values of tt$_H$, tt$_V$, ω_H and ω_V were generally calibrated for a single vegetation type over the different experiments and different measurement configurations. For instance the same values tt$_H$=2, tt$_V$=1 and $\omega_H=\omega_V=0.05$ were calibrated for corn over the BARC (// and ⊥), REBEX and EMIRAD-2001 (// and ⊥) data sets. Also, the values tt$_H$=2, tt$_V$=1 or 2 and $\omega_H=\omega_V=0$ were calibrated for soybean over the BARC (// and ⊥) and PORTOS-91 data sets. No effects of polarization on ω_P could be noted ($\omega_H=\omega_V$ for all data sets). Calibrated ω is low generally: $\omega=0$ was obtained for wheat and soybean and a higher value of ω was obtained for corn ($\omega=0.05$). The calibrated value of optical depth was generally found to be sensitive to incidence angle and polarization. The case tt$_H$=1 and tt$_V$=1, which corresponds to isotropic attenuation effects within the vegetation, was obtained only for soybean with the BARC data set. Anisotropic effects were obtained for corn over all data sets (tt$_H$=2, corresponding to slightly increasing values of τ_H with θ) and for wheat (tt$_V$=8, corresponding to a strong increase of τ_V with θ).

Using the retrieved value of τ_{NAD} and ground measurements of V_{WC} and LAI, the slope, intercept and R^2 of the linear regression between τ_{NAD} vs. V_{WC} and τ_{NAD} vs. LAI could be computed. They are given in Table 5. These two relationships are illustrated for PORTOS-91 in Figs. 4 and 5. If we consider the relationship $\tau_{NAD}(V_{WC})$, the value of the intercept is generally very low. This is a direct result from minimizing the intercept, as this was one of the criteria used to calibrate the soil and vegetation parameters. Therefore, the slope is very close to the b parameter, traditionally used to compute τ_{NAD} as $\tau_{NAD}=b \cdot V_{WC}$, and will be referred to as b in the following. The average value of

b is generally found to be close to 0.15 for crops (Jackson & Schmugge, 1991). In this study, the value of b was found to be strongly dependent on the crop type: very low and consistent values were obtained for corn ($b \sim 0.044$ for REBEX, 0.050 for EMIRAD-2001 and ~ 0.070 for BARC) and for wheat ($b \approx 0.077$). Much higher values were obtained for soybean: $b=0.174$ for PORTOS-91 and $b \sim 0.17$ for BARC (// and ⊥). It is likely that the relatively low values of the ratio $b=\tau_{NAD}/V_{WC}$ for corn and wheat can be related to the vertical stems. These stems have low attenuation effects at nadir (and more generally at H polarization), but correspond to a strong contribution in the vegetation water content (Hornbuckle et al., 2003; Wigneron et al., 1995).

Parameters of the linear regression between retrieved τ_{NAD} vs. LAI are also given in Table 5, except for the BARC data set, in which no LAI data were available (b'_S and b''_S correspond to the
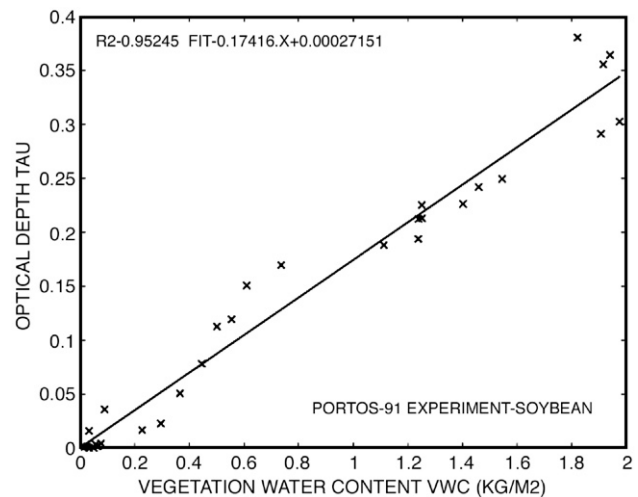
Fig. 4. PORTOS-91: comparison between retrieved τ_{NAD} and measured V_{WC} (kg/m^2).
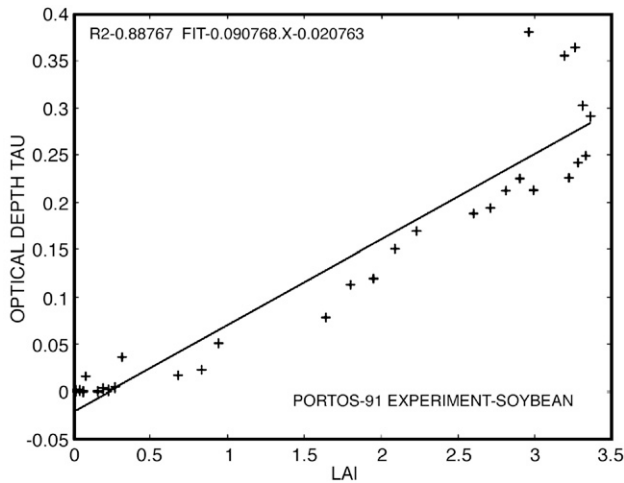
Fig. 5. PORTOS-91: comparison between retrieved τ_{NAD} and measured LAI (m²/m²).

slope and intercept of this regression). It was found that the value of the intercept (b''_S) is generally very low and the slope (b'_S) is strongly dependent on the crop type: b'_S varies from 0.034 for wheat to 0.090 for soybean. A medium value, $b'_S \approx 0.047$ was obtained for corn. Except for PORTOS-93 (all_the_data), that includes observations over an altered and senescent canopy structure, a high correlation is generally found between retrieved τ_{NAD} and LAI.

5. Discussion and conclusion

L-MEB is the forward model used in the SM Level-2 retrieval algorithm currently being developed for SMOS. This model will be one of the main reference models which will be used for inversion and assimilation studies of the SMOS observations. In the algorithm process, the SMOS observations are computed with the L-MEB model accounting for the different vegetation types included in the SMOS footprint for each incidence angle. The first objective of this study was to describe L-MEB in detail.

The second objective of this study was to calibrate the model for a variety of cropped fields. L-MEB was used in a study investigating soil moisture retrievals. A '3-Parameter' inversion method, in which S_M, τ_{NAD} and H_R were retrieved simultaneously, was implemented. Soil and vegetation model parameters were calibrated over five data sets including multi-angular L-band microwave observations and detailed information on the soil and vegetation variables.

Many parameters were tuned in the '3-P' scheme so that very good SM retrievals could be obtained in theory. However, the calibrated values of the model parameters were realistic and made us confident in the fact the proposed method can be operational. First, these calibrated values were found to be quite consistent with the information which was available about the soil and vegetation characteristics:

– similar values of H_R were obtained over all crops with relatively smooth soils ($H_R \sim 0.1$) and these values were

consistent with many previous studies (Jackson et al., 1999). About the same values of H_R were obtained over corn at the BARC and REBEX sites ($H_R \sim 0.5$). This value is also consistent with higher roughness effects due to irrigation rows at the soil surface over these two sites, while corn was irrigated with sprinklers at the INRA site.
– the calibration of N_{RV} and N_{RH} is in general quite consistent with results obtained from the large SMOS-REX data set over bare soil ($N_{RV}=-1$ or 0 and $N_{RH}=0$ or 1; Escorihuela et al., submitted for publication).

Very consistent results were also obtained for vegetation since the same values of the vegetation parameters were generally calibrated for a single vegetation type over the different experiments and different measurement configurations:

– the same value of ω_P was obtained for the three corn fields ($\omega_P=0.05$), while ω_P could be considered as negligible for all the other crop types (this is consistent with many previous studies).
– Retrieved values of tt_V and tt_H are consistent with results from physical models (Ferrazzoli et al., 2000; Wigneron et al., 1993a) over wheat ($tt_v=8$) and soybean (an almost isotropic canopy so that $tt_V \sim tt_H \sim 1$).

Interesting new results about the b parameter were obtained in this study: much lower values of b were obtained in comparison with previous studies (Wigneron et al., 2004) and these values strongly depend on the crop type. The fact that different values of b were obtained can be probably related to the fact that the sensitivity of optical depth on polarization and incidence angle (θ) was accounted for in this study (through the terms tt_H and tt_V). Also, the modelling of soil (through the terms H_R, N_{RV} and N_{RH}) was much improved in L-MEB in comparison with previous analyses. Although large values of b were obtained over soybean ($b \sim 0.17$), the value of b was generally found to be low: about 0.075 over wheat and 0.06 for corn, while values close to 0.1 or 0.15 were generally reported in the literature. Note that the values of b given in this study correspond to nadir estimations of optical depth (τ_{S-NAD}). Considering the effects of tt_H and tt_V, the optical depth strongly increases as a function of incidence angle at V polarization over wheat ($tt_V=8$) and at H polarization over corn ($tt_H=2$). Conversely, values of b reported in the literature are generally average values based on T_B measurements made at various incidence angles (Van de Griend & Wigneron, 2004). The low values of b over corn are in good agreement with results obtained by Hornbuckle and England (2004) who noted that the radiometric sensitivity to soil moisture at 1.4 GHz through a corn canopy at a maximum biomass was much higher than expected. All these recent results suggest that a larger range in the values of b at nadir, from 0.05 to 2, should be considered for crops which do not include a litter layer. New combined experimental and modelling researches are probably necessary to investigate more in depth the large variability of b over a variety of crop types.

New results describing the relationship between nadir optical depth and LAI were also given for three vegetation types (wheat, soybean and corn). The results showed that the correlation between τ_{NAD} and LAI was quite good generally over all crop types. These results are quite important and helpful to justify the fact that LAI was the variable selected to initialize the value of τ_{NAD} in the SM L-2 algorithm.

The 3-Parameter method was found to be the best for SM retrievals over the homogeneous covers considered in this study. How do the uncertainties on the model parameters may affect the retrievals for operational applications? In the '3P' approach, soil moisture and optical depth are unknowns, while an estimate of the roughness parameter H_R is required with a relatively good accuracy ($\sigma(H_R) = 0.1$) and all the other soil and vegetation parameters (H_R, N_{RV},....) are assumed to be known and should be calibrated prior to the SM inversion. Among all these soil and vegetation parameters, H_R is the parameter whose calibration has probably the larger impact on the SM retrieval accuracy. Uncertainties on the calibrated values of N_{RH} and N_{RV} are relatively low (their variability is relatively low over a large range of roughness conditions as shown before). Conversely, the value of H_R should be known with a relatively good accuracy. For instance, considering the value of H_R over corn is the same as that of soybean (i.e. using a value $H_R = 0.1$ instead of 0.6) might lead to errors of about 0.07 m^3/m^3 in the retrieved SM value. However, it is likely that the H_R values obtained over the smooth soybean field and the rough corn field correspond to relatively "extreme" local roughness conditions and that the variability in the roughness characteristics are lower at a larger scale. At the scale of 1 or 4 km, which is used in the Level 2 algorithm to define maps of vegetation classes and roughness properties, the effective H_R values result from the mixing effects of a variety of local roughness conditions, so that these values might be relatively constant from one geographical location to the other.

Although uncertainties on the calibrated values of the vegetation parameters have mainly an impact on the value of the retrieved optical depth, they also have an impact on the retrieved SM, but to a lower extent than H_R. Over heterogeneous pixels, the fact that the b parameter may depend strongly on the vegetation type may have a negative impact since an accurate mapping of the different vegetation types – and of the associated b, b'_S and b''_S values – could be required in the retrieval algorithm.

However, as discussed for H_R, it is likely that the differences in the b values (b varies from about 0.05 for corn to about 0.2 for soybean) obtained at local scale between crop types with very different vegetation structures correspond to extreme cases. These cases may not be really representative of the variability of b at a larger spatial scale. At a larger scale (1 km or higher), the b parameters are computed as average values over a mixture of local vegetation conditions (in terms of canopy types and structure). As there is a large variability in the b values at a very local scale (less than 100 m), these average values of b are probably relatively stable from one location to the other.

This discussion can be related to the conclusions of Cognard et al. (1995) in the active domain, who found there was a large

variability in the local (field) vegetation and roughness conditions over an hydrological test site in Brittany. At a larger scale (the whole watershed), these local effects were averaged so that the relationship between SM and the backscattering coefficient was found to be much more clear and robust than at local scale.

Future studies based on measurements over mixed pixels at a larger scale (about 1 to 5 km) will be very helpful to confirm these hypotheses made on the roughness and vegetation model parameters. These studies will be based on experiments including airborne measurements at a regional scale, such as the NAFE campaign in Australia (Walker et al., 2006). This airborne data set will also be very useful to extend the present results over natural covers and prairies including a litter.

References

Brunfeldt, D. R., & Ulaby, F. T. (1984). Measured microwave emission and scattering in vegetation canopies. *IEEE Transactions on Geoscience and Remote Sensing*, 22, 520−524.

Chen, K. S., Wu, T. D., Tsang, L., Li, Q., Shi, J., & Fung, A. K. (2003). Emission of rough surfaces calculated by the integral equation method with comparison to three-dimensional moment method simulations. *IEEE Transactions on Geoscience and Remote Sensing*, 41(1), 90−101.

Choudhury, B. J., Schmugge, T. J., Chang, A., & Newton, R. W. (1979). Effect of surface roughness on the microwave emission from soils. *Journal of Geophysical Research*, 84, 5699−5706.

Choudhury, B. J., Schmugge, T. J., & Mo, T. (1982). A parameterization of effective soil temperature for microwave emission. *Journal of Geophysical Research*, 87(C2), 1301−1304.

Cognard, A. -L., Loumagne, C., Normand, M., Olivier, P., Ottlé, C., Vidal-Madjar, D., et al. (1995). Evaluation of the ERS 1/synthetic aperture radar capacity to estimate surface soil moisture: Two-year results over the Naizin watershed. *Water Resources Research*, 31(4), 975−982.

Della Vecchia, A., Ferrazzoli, P., Giorgio, F., and Guerriero, L. (in press). A large scale approach to estimate L band emission from forest covered surfaces, In Proceedings of the 2nd International Symposium on Recent Advances in Quantitative Remote Sensing, Torrent (Valencia, Spain), 25–29 Sept., 2006.

Della Vecchia, A., Saleh, K., Ferrazzoli, P., Guerriero, L., & Wigneron, J. -P. (2006, July). Simulating L-Band emission of coniferous forests using a discrete model and a detailed geometrical representation. *IEEE Transactions on Geoscience and Remote Sensing Letters*, 3(3), 364−368.

De Rosnay, P., Calvet, J. -C., Kerr, Y., Wigneron, J. -P., Lemaitre, F., Escorihuela, M. -J., et al. (2006a). SMOSREX: A long term field campaign experiment for soil moisture and land surface processes remote sensing. *Remote Sensing of Environment*, 102, 377−389.

De Rosnay, P., Wigneron, J. -P., Holmes, T., & Calvet, J. -C. (2006b). Parameterizations of the effective temperature for L-band radiometry. Intercomparison and long term validation with SMOSREX field experiment. In C. Mätzler, P. W. Rosenkranz, A. Battaglia, & J. P. Wigneron (Eds.), *Thermal Microwave Radiation- Applications for Remote Sensing* (pp. 312−324). London, UK: IEE Electromagnetic Waves Series.

Dirmeyer, P., & Gao, G. (2004, Sept). A Status Report on the Second Global Soil Wetness Project GSWP-2, Center for Ocean-Land-Atmosphere Studies Calverton. Maryland, USA. www.iges.org/glass/GSWP_status

Dobson, M. C., Ulaby, F. T., Hallikainen, M. T., & El-Reyes, M. A. (1985). Microwave dielectric behavior of wet soil- Part II: Dielectric mixing models. *IEEE Transactions on Geoscience and Remote Sensing*, 23, 35−46.

Entekhabi, D., Njoku, E. G., Houser, P., Spencer, M., Doiron, T., Kim, Y., et al. (2004). The hydrosphere state (Hydros) satellite mission: An Earth system pathfinder for global mapping of soil moisture and land freeze/thaw. *IEEE Transactions on Geoscience and Remote Sensing*, 42(10), 2184−2195.

Escorihuela, M. J., Kerr, Y., de Rosnay, P., Wigneron, J. -P., Calvet, J. -C., & Lemaître, F. (submitted for publication). A Simple model of the bare soil microwave emission at L-Band. *IEEE Transactions on Geoscience and Remote Sensing*.

Fenollar, J., Saleh, K., Balling, J. E., Søbjærg, S. S., Skou, N., Wigneron, J. -P., et al. (2006). The MELBEX (Mediterranean Ecosystem L-band Characterisation Experiment) Experiment in the context of the ESA SMOS (Soil Moisture and Ocean Salinity) Mission. Assembly of Geodesy and Geophysics. http://www-5ahlgg.inm.es University of Sevilla, 30 Jan– 3 Feb, 2006.

Ferrazzoli, P., & Guerriero, L. (1996). Passive microwave remote sensing of forests: A model investigation. *IEEE Transactions on Geoscience and Remote Sensing*, 34, 433−443.

Ferrazzoli, P., Guerriero, L., & Wigneron, J. -P. (2002). Simulating L-band emission of forests in view of future satellite applications. *IEEE Transactions on Geoscience and Remote Sensing*, 40(12), 2700−2708.

Ferrazzoli, P., Wigneron, J. -P., Guerriero, L., & Chanzy, A. (2000). Multifrequency emission of wheat: Modeling and applications. *IEEE Transactions on Geoscience and Remote Sensing*, 38, 2598−2607.

Grant, J. P., Wigneron, J. -P., Van de Griend, A. A., Schmidl Søbjærg, S., Skou, N., & Balling, J. (2007). Bray-2004 L-band radiometric field experiment in the Les Landes forest: microwave signal behaviour for varying conditions of ground moisture. *Remote Sensing of Environment*, 107, 639−655.

Guglielmetti, M., Schwank, M., Mätzler, C., Oberdörster, C., Vanderborght, J., & Flühler, H. (submitted for publication). Measured Microwave Radiative Transfer Properties of a Deciduous Forest Canopy. *Remote Sensing of Environment*.

Hallikainen, M., Ulaby, F., Dobson, M., & El-Rayes, M. (1984). Dielectric measurements of soils in the 3- to 37- GHz band between −50 °C and 23 °C. *IGARSS'84, Strasbourg France* (pp. 163−168).

Hallikainen, M., Ulaby, F., Dobson, M., El-Rayes, M., & Wu, F. (1985). Microwave dielectric behavior of wet soil- Part I: Empirical models and experimental observations. *IEEE Transactions on Geoscience and Remote Sensing*, 23(1), 25−34.

Holmes, T. R. H., de Rosnay, P., de Jeu, R., Wigneron, J. -P., Kerr, Y., Calvet, J. -C., et al. (2006). A new parameterization of the effective temperature for L band radiometry. *Geophysical Research Letters*, 33, L07405. doi:10.1029/2006GL025724

Hornbuckle, B. K., & England, A. W. (2004). Radiometric sensitivity to soil moisture at 1.4 GHz through a corn crop at maximum biomass. *Water Ressources Research*, 40(10). doi:10.1029/2003WR002931

Hornbuckle, B. K., & England, A. W. (2005). Diurnal variation of vertical temperature gradients within a field of maize: Implications for satellite microwave radiometry. *IEEE Geoscience and Remote Sensing Letters*, 2(1), 74−77.

Hornbuckle, B. K., England, A. W., Anderson, M. C., Viner, B. (in press). The effect of free water in a maize canopy on microwave emission at 1.4 GHz. *Agricultural and Forest Meteorology*.

Hornbuckle, B. K., England, A. W., De Roo, R. D., Fischman, M. A., & Boprie, D. L. (2003). Vegetation canopy anisotropy at 1.4 GHz. *IEEE Transactions on Geoscience and Remote Sensing*, 41, 2211−2222.

Jackson, T. J., Chen, D., Cosh, M., Li, F., Anderson, M., Walthall, C., et al. (2004). Vegetation water content mapping using Landsat data derived normalized difference water index for corn and soybeans. *Remote Sensing of Environment*, 92, 475−482.

Jackson, T. J., Le Vine, D. M., Hsu, A. Y., Oldak, A., Starks, P. J., Swift, C. T., et al. (1999). Soil moisture mapping at regional scales using microwave radiometry: the Southern Great Plains Hydrology Experiment. *IEEE Transactions on Geoscience and Remote Sensing*, 37, 2136−2150.

Jackson, T. J., & Schmugge, T. J. (1991). Vegetation effects on the microwave emission of soils. *Remote Sensing of Environment*, 36, 203−212.

Kerr, Y.H. (in press). Soil moisture from Space: Where are we? *Hydrogeology Journal*.

Kerr, Y. H., & Njoku, E. G. (1990). A semiempirical model for interpreting microwave emission from semiarid land surfaces as seen from space. *IEEE Transactions on Geoscience and Remote Sensing*, 28, 384−393.

Kerr, Y., Sécherre, F., Lastenet, J., & Wigneron, J. -P. (2003). SMOS: Analysis of perturbing effects over land surfaces. *Proceedings of IEEE Int. Geosci. Remote Sens. Symp. (IGARSS'03), Jul. 21-25 Toulouse, France*.

Kerr, Y. H., Waldteufel, P., Richaume, P., Davenport, I., Ferrazzoli, P., & Wigneron, J. -P. (2006). *SMOS level 2 processor Soil moisture Algorithm theoretical Basis Document (ATBD)*. SM-ESL (CBSA), CESBIO, Toulouse, SO-TN-ESL-SM-GS-0001, V5.a, 15/03/2006.

Kerr, Y. H., Waldteufel, P., Wigneron, J. -P., Font, J., & Berger, M. (2001). Soil moisture retrieval from space: The Soil Moisture and Ocean Salinity (SMOS) Mission. *IEEE Transactions on Geoscience and Remote Sensing*, 39(8), 1729−1735.

Lopez-Baeza, E., Calvet, J. -C., Etcheto, J., Finkenzeller, H., Font, J., Kerr, Y., et al. (2003). *EuroSTARRS: campaign description, SP-525: First Results Workshop of EuroSTARRS, WISE, LOSAC, 4-6 Nov* (pp. 37−47). Noordwijk, The Netherlands: ESA Pub. Div., ESTEC.

Macelloni, G., Brogioni, M., Pampaloni, P., Cagnati, A., & Drinkwater, M. R. (2006). DOMEX 2004: An experimental campaign at Dome-C Antarctica for the calibration of spaceborne low-frequency microwave radiometers. *IEEE Transactions on Geoscience and Remote Sensing*, 44(10), 2642−2653.

Masson, V., Champeau, J. -L., Chauvin, F., Meriguet, C., & Lacaze, R. (2003). A global data base of land surface parameters at 1 km resolution in meteorological and climate models. *Journal of Climate*, 16, 1261−1282.

Mätzler, C. (1993). *Passive microwave signature catalog 1989–1992 (Vol.1)*. IAP-Report, University of Bern, Feb. (1993), Vol 2. May 1994, Vol 3, July (1994).

Mätzler, C. (1998). Microwave permittivity of dry sand. *IEEE Transactions on Geoscience and Remote Sensing*, 36, 317−319.

Mätzler, C. (2001). Applications of SMOS over terrestrial ice and snow, 3rd SMOS Workshop, Munich, Germany, Dec., 2001. http://www.cesbio.ups-tlse.fr/data_all/SMOS_WS/WS3/liste.htm

Mätzler, C., Rosenkranz, P. W., Battaglia, A., & Wigneron, J. -P. (2006). *Thermal Microwave Radiation — Applications for Remote Sensing*. IET Electromagnetic Waves Series 52. London, UK, 555 pp.

Mo, T., Choudhury, B. J., Schmugge, T. J., Wang, J. R., & Jackson, T. J. (1982). A model for microwave emission from vegetation-covered fields. *Journal of Geophysical Research*, 87, 11.229−11.237.

Mo, T., & Schmugge, T. J. (1987). A parameterization of the effect of surface roughness on microwave emission. *IEEE Transactions on Geoscience and Remote Sensing*, 25, 47−54.

Njoku, E. G., Jackson, T. J., Lakshmi, V., Chan, T. K., & Nghiem, S. V. (2003). Soil moisture retrieval from AMSR-E. *IEEE Transactions on Geoscience and Remote Sensing*, 41(2), 215−229.

Njoku, E. G., & Li, L. (1999). Retrieval of land surface parameters using passive microwave measurements at 6–18 GHz. *IEEE Transactions on Geoscience and Remote Sensing*, 37(1), 79−93.

Noilhan, J., & Planton, S. (1989). A simple parameterization of land surface processes for meteorological models. *Monthly Weather Review*, 117, 536−549.

Owe, M., de Jeu, R., & Walker, J. (2001). A methodology for surface soil moisture and vegetation optical depth retrieval using the microwave polarization difference index. *IEEE Transactions on Geoscience and Remote Sensing*, 39(8), 1643−1654.

Pampaloni, P., & Paloscia, S. (1986). Microwave emission and plant water content: A comparison between field measurements and theory. *IEEE Transactions on Geoscience and Remote Sensing*, 24, 900−905.

Pardé, M., Wigneron, J. -P., Chanzy, A., Kerr, Y., Calvet, J. C., Waldteufel, P., et al. (2004). N-Parameter retrievals from L-band microwave measurements over a variety of agricultural crops. *IEEE Transactions on Geoscience and Remote Sensing*, 42(6), 1168−1178.

Pellarin, T., Calvet, J. -C., & Wigneron, J. -P. (2003b). Surface soil moisture retrieval from L-band radiometry: A global regression study. *IEEE Transactions on Geoscience and Remote Sensing*, 41(9), 2037−2051.

Pellarin, T., Kerr, Y. H., & Wigneron, J. -P. (2006). Global simulation of brightness temperatures at 6.6 and 10.7 GHz over land based on SMMR data set analysis. *IEEE Transactions on Geoscience and Remote Sensing*, 44(9), 2492−2505.

Pellarin, T., Wigneron, J. -P., Calvet, J. -C., Ferrazzoli, P., Douville, H., Lopez-Baeza, E., et al. (2003a). Two-Year global simulation of L-band brightness temperatures over land. *IEEE Transactions on Geoscience and Remote Sensing*, 41(9), 2135−2139.

Pellarin, T., Wigneron, J. -P., Calvet, J. -C., & Waldteufel, P. (2003c). Global soil moisture retrieval from a synthetic L-band brightness temperature data set. *Journal of Geophysical Research*, 108(D12), 4364. doi:10.1029/2002JD003086

Prigent, C., Wigneron, J. -P., Rossow, W. B., & Pardo-Carrion, J. R. (2000). Frequency and angular variations of land surface microwave emissivities: Can we estimate SSM/T and AMSU emissivities from SSM/I emissivities? *IEEE Transactions on Geoscience and Remote Sensing*, 38, 2373−2386.

Pulliainen, J., & Hallikainen, M. (2001). Retrieval of regional snow water equivalent from space-borne passive microwave observations. *Remote Sensing of Environment*, 75, 76−85.

Putuhena, W., & Cordery, I. (1996). Estimation of interception capacity of the forest floor. *Journal of Hydrology*, 182, 283−299.

Raju, S., Chanzy, A., Wigneron, J. -P., Calvet, J. -C., Kerr, Y., & Laguerre, L. (1995). Soil-moisture and temperature profile effects on microwave emission at low-frequencies. *Remote Sensing of Environment*, 54, 85−97.

Saleh, K., Wigneron, J. P., Calvet, J. C., Lopez-Baeza, E., Berger, M., Wursteisen, P., et al. (2004). The EuroSTARRS airborne campaign in support of the SMOS mission: First results over land surfaces. *International Journal of Remote Sensing*, 25(1), 177−194.

Saleh, K., Wigneron, J. -P., de Rosnay, P., Calvet, J. -C., Escorihuela, M. -J., Kerr, Y., et al. (2006a). Impact of rain interception by vegetation and mulch on the L-band emission of natural grass. *Remote Sensing of Environment*, 101, 127−139.

Saleh, K., Wigneron, J. -P., de Rosnay, P., Calvet, J. -C., & Kerr, Y. (2006b). Semi-empirical regressions at L-band applied to surface soil moisture retrievals over grass. *Remote Sensing of Environment*, 101, 415−426.

Saleh, K., Wigneron, J. -P., Waldteufel, P., de Rosnay, P., Schwank, M., Calvet, J. -C., Kerr, Y. (submitted for publication). Estimates of surface soil moisture over grass covers using L-band radiometry. *Remote Sensing of Environment*, submitted.

Schmugge, T. (1998). Applications of passive microwave observations of surface soil moisture. *Journal of Hydrology*, 212–213, 188−197.

Schmugge, T. J., Wang, J. R., & Asrar, G. (1988). Results from the push broom microwave radiometer flights over the Konza Prairie in 1985. *IEEE Transactions on Geoscience and Remote Sensing*, 26, 590−597.

Schneeberger, K., Schwank, M., Stamm, C., de Rosnay, P., Mätzler, C., & Fluhler, H. (2004). Topsoil structure influencing soil water retrieval by microwave radiometry. *Vadose Zone Journal*, 3, 1169−1179.

Schwank, M., & Mätzler, C. (2006). Air-to-soil transition model. In C. Mätzler, P. W. Rosenkranz, A. Battaglia, & J. P. Wigneron (Eds.), *Thermal microwave radiation — Applications for remote sensing* (pp. 287−301). London, UK: IEE Electromagnetic Waves Series.

Schwank, M., Mätzler, M., Guglielmetti, M., & Fluhler, H. (2005, October). L-Band radiometer measurements of soil water under growing clover grass. *IEEE Transactions on Geoscience and Remote Sensing*, 43(10), 2225−2237.

Schwank, M., Stähli, M., Wydler, H., Leuenberger, J., Mätzler, C., & Hannes, F. (2004). Microwave L-band emission of freezing soil. *IEEE Transactions on Geoscience and Remote Sensing*, 42(6), 1252−1261.

Seuffert, G., Wilker, H., Viterbo, P., Mahfouf, J. -F., Drusch, M., & Calvet, J. -C. (2003). Soil moisture analysis combining screen-level parameters and microwave brightness temperature: A test with field data. *Geophysical Research Letters*, 30(10). doi:10.1029/2003GL017128

Shi, J., Chen, K. S., Li, Q., Jackson, T. J., O'Neill, P. E., & Tsang, L. (2002). A parameterized surface reflectivity model and estimation of bare-surface soil moisture with L-band radiometer. *IEEE Transactions on Geoscience and Remote Sensing*, 40(12), 2674−2686.

Shi, J. C., Jiang, L. M., Zhang, L. X., Chen, K. S., Wigneron, J. -P., & Chanzy, A. (2005, December). A parameterized multi-frequency-polarization surface emission model. *IEEE Transactions on Geoscience and Remote Sensing*, 43(12), 2821−2831.

Stiles, J. M., Sarabandi, K., & Ulaby, K. T. (2000). Electromagnetic scattering from grassland-Part II: Measurement and modeling results. *IEEE Transactions on Geoscience and Remote Sensing*, 38, 349−356.

Ulaby, F. T., Moore, R. K. & Fung, A. K. (1981–1986). *Microwave Remote Sensing — Active and Passive*, vol I, II, 1981−82, Addison-Wesley Publishing Company; vol III, 1986, Artech House, Norwood, MA.

Ulaby, F. T., & Wilson, E. A. (1985). Microwave attenuation properties of vegetation canopies. *IEEE Transactions on Geoscience and Remote Sensing*, 23, 746−753.

Van de Griend, A. A., & Owe, M. (1993). Determination of microwave vegetation optical depth and single scattering albedo from large scale soil moisture and Nimbus/SMMR satellite observations. *International Journal of Remote Sensing*, 14(10), 1875−1886.

Van de Griend, A. A., & Wigneron, J. -P. (2004). The b-factor as a function of frequency and canopy type at H polarization. *IEEE Transactions on Geoscience and Remote Sensing*, 42(4), 786−794.

Walker, J. P., Merlin, O., Panciera, R., & Kalma, J. D. (2006, 4–8 December). National airborne field experiments for soil moisture remote sensing. *30th hydrology and water resources symposium [CD-ROM]* Launceston, Australia: The Institute of Engineers Australia.

Wang, J. R., & Choudhury, B. J. (1981). Remote sensing of soil moisture content over bare field at 1.4 GHz frequency. *Journal of Geophysical Research*, 86, 5277−5282.

Wang, J. R., O'Neill, P. E., Jackson, T. J., & Engman, E. T. (1983). Multifrequency measurements of the effects of soil moisture, soil texture, and surface roughness. *IEEE Transactions on Geoscience and Remote Sensing*, 21, 44−51.

Wang, J. R., & Schmugge, T. J. (1980). An empirical model for the complex dielectric permittivity of soils as a function of water content. *IEEE Transactions on Geoscience and Remote Sensing*, 18(4), 288−295.

Wang, J. R., Schmugge, T., Gould, W., Fuchs, J., Glazer, W., & McMurtrey, J. E. (1982). A multi-frequency radiometric measurement of soil moisture content over bare and vegetation fields. *Geophysical Research Letters*, 9(4), 416−419.

Wegmüller, U., & Mätzler, C. (1999). Rough bare soil reflectivity model. *IEEE Transactions on Geoscience and Remote Sensing*, 37, 1391−1395.

Wigneron, J. -P., Calvet, J. -C., & Kerr, Y. (1996). Monitoring water interception by crop fields from passive microwave observations. *Agricultural and Forest Meteorology*, 80, 177−194.

Wigneron, J. -P., Calvet, J. -C., Kerr, Y. H., Chanzy, A., & Lopes, A. (1993a). Microwave emission of vegetation: Sensitivity to leaf characteristics. *IEEE Transactions on Geoscience and Remote Sensing*, 31, 716−726.

Wigneron, J. -P., Calvet, J. -C., Pellarin, T., Van de Griend, A., Berger, M., & Ferrazzoli, P. (2003). Retrieving near surface soil moisture from microwave radiometric observations: Current status and future plans. *Remote Sensing of Environment*, 85, 489−506.

Wigneron, J. -P., Chanzy, A., Calvet, J. -C., & Bruguier, N. (1995). A simple algorithm to retrieve soil moisture and vegetation biomass using passive microwave measurements over crop fields. *Remote Sensing of Environment*, 51, 331−341.

Wigneron, J. -P., Chanzy, A., Calvet, J. -C., Olioso, A., & Kerr, Y. (2002). Modeling approaches to assimilating L-band passive microwave observations over land surfaces. *Journal of Geophysical Research*, 107, D14. doi:10.1029/2001JD000958

Wigneron, J. -P., Kerr, Y. H., Chanzy, A., & Jin, Y. Q. (1993b). Inversion of surface parameters from passive microwave measurements over a soybean field. *Remote Sensing of Environment*, 46, 61−72.

Wigneron, J.-P., Kerr, Y., Waldteufel, P., et al. (in press). Recent Advances in modelling the land surface emission at L-band- Application to L-MEB in the operational SMOS algorithm, In Proceedings of the International Symposium on Recent Advances in Remote Sensing (RAQRS'2006), 25–29 Sept., 2006, Torrent,Valencia.

Wigneron, J. -P., Laguerre, L., & Kerr, Y. (2001). Simple modeling of the L-band microwave emission from rough agricultural soils. *IEEE Transactions on Geoscience and Remote Sensing*, 39(8), 1697−1707.

Wigneron, J. -P., Pardé, M., Waldteufel, P., Chanzy, A., Kerr, Y., Schmidl, S., et al. (2004). Characterizing the dependence of vegetation parameters on crop type, view angle and polarization at L-Band. *IEEE Transactions on Geoscience and Remote Sensing*, 42(2), 416−425.

Wigneron, J. -P., Pellarin, T., Calvet, J. -C., de Rosnay, P., Saleh, K., & Kerr, Y. (2006a). L-MEB: A simple model at L-band for the continental areas — Application to the simulation of a half-degree resolution and global scale data set. In C. Mätzler, P. W. Rosenkranz, A. Battaglia, & J. P. Wigneron (Eds.), *Thermal microwave radiation — applications for remote sensing* (pp. 362−371). London, UK: IEE Electromagnetic Waves Series.

Wigneron, J. -P., Shi, J. C., Escorihuela, M. -J., & Chen, K. -S. (2006b). Modeling the soil microwave emission. In C. Mätzler, P. W. Rosenkranz, A. Battaglia, & J. P. Wigneron (Eds.), *Thermal microwave radiation-applications for remote sensing* (pp. 276−287). London, UK: IEE Electromagnetic Waves Series.

Wigneron, J. -P., Waldteufel, P., Chanzy, A., Calvet, J. -C., & Kerr, Y. (2000). Two-D microwave interferometer retrieval capabilities of over land surfaces (SMOS Mission). *Remote Sensing of Environment*, *73*, 270−282.